Elucidating the interplay between structure and electrochemical behavior in lignin-based polymer electrolytes for potassium batteries

Battery Energy

WILEY

BATTERY ENERGY Open Access

RESEARCH ARTICLE OPEN ACCESS

Elucidating the Interplay Between Structure and Electrochemical Behavior in Lignin-Based Polymer Electrolytes for Potassium Batteries

Giuseppe Pascuzzi[1] | Sabrina Trano[2] | Carlotta Francia[2] | Stefano Turri[1] | Federico Bella[2] | Gianmarco Griffini[1]

[1]Department of Chemistry, Materials and Chemical Engineering "Giulio Natta", Politecnico di Milano, Milano, Italy | [2]Department of Applied Science and Technology, Politecnico di Torino, Torino, Italy

Correspondence: Federico Bella (federico.bella@polito.it) | Gianmarco Griffini (gianmarco.griffini@polimi.it)

Received: 8 October 2024 | **Revised:** 7 January 2025 | **Accepted:** 25 January 2025

Funding: This work was supported by Horizon 2020 Framework Programme (grant agreement no. 952941, project BIOMAC), Ministero dell'Università e della Ricerca (FISA-2022-00983), European Union Next-GenerationEU (Agritech National Research Center, cn00000022), and Regione Lombardia (EcoCIRC Regional Hub).

Keywords: bio-based polymers | gel polymer electrolyte | lignin | postlithium batteries | potassium batteries | sustainable batteries

ABSTRACT

Potassium batteries are very appealing for stationary applications and domestic use, offering a promising alternative to lithium-ion systems. To improve their safety and environmental impact, gel polymer electrolytes (GPEs) based on bioderived materials can be employed. In this work, a series of biobased membranes are developed by crosslinking pre-oxidized Kraft lignin as bio-based component and poly(ethylene glycol) diglycidyl ether (PEGDGE) as functional linker with 200, 500, and 1000 g mol^{-1} molecular weight. The influence of PEGDGE chain length on the physicochemical properties and electrochemical performance of GPEs for potassium batteries is investigated. These membranes exhibit thermal stability above 240°C and tunable glass transition temperatures depending on the PEGDGE molecular weight. Their mechanical properties are determined by rheology measurements in dry and swollen states, evidencing a slight decrease of elastic modulus (G′) by increasing PEGDGE chain length. An approximately one-order-of-magnitude lower G′ value is observed in swollen membranes versus their dry counterpart. Upon successful activation of the lignin-based membranes by swelling in the liquid electrolyte embedding potassium salts, these GPEs are tested in potassium metal cell prototypes. These systems exhibit ionic conductivity of ~10^{-3} S cm^{-1} at ambient temperature. Interestingly, battery devices equipped with the GPE based on PEGDGE 1000 g mol^{-1} withstand current densities as high as 1.5 mA cm^{-2} during operation. Moreover, the same devices reach specific capacities of 130 mAh g^{-1} at 0.05 A g^{-1} in the first 100 cycles and long-term operation for over 2500 cycles, representing outstanding achievements as bio-sourced systems for potassium batteries.

1 | Introduction

The constant technological development experienced by human society in the past century has been steadily accompanied by an increasing demand for widely available and reliable energy sources, among which electrical energy plays a pivotal role [1–3]. To address this issue at a global scale without compromising the ecosystem, the past few decades have been characterized by intensive research efforts in the development of efficient energy conversion technologies of limited environmental impact and

Giuseppe Pascuzzi and Sabrina Trano contributed equally to this study.

ready scalability. Among them, those based on renewable sources such as solar, wind, geothermal, and tidal energy have become the subject of intensive studies both from academia and industry [4, 5]. While potentially being able to provide a virtually unlimited (on a human timescale) and readily accessible energy for direct use, all these natural approaches are characterized by an intrinsically discontinuous availability, which makes their output variable and uncontrollable over time and geographical location [6, 7]. For these reasons, efficient energy storage systems are highly desirable to make such intermittent energy sources geographically distributed and potentially available when required, thus providing a solution for power grid integration and remote/delocalized energy distribution [2, 8].

Among the different energy storage technologies available today for combination with renewable energy conversion systems [9, 10], electrochemical energy storage represents one of the most advantageous solutions to meet the constantly growing demand for portable energy devices. In this category, rechargeable batteries are extensively employed for a wide range of storage applications, including small-scale and large-scale utilization, transportation, and stationary grid storage, and they are playing a key role as enablers of the transition toward more widespread use of renewable energy on the global landscape [11, 12].

In this context, lithium-ion batteries (LIBs) are the most popular solution for portable electronics, automotive applications, and stationary purposes, and their demand keeps growing globally as a result of their versatility and ability to provide high voltage, high specific energy, and high energy density with long cycles life [13–15]. However, issues related to the limited availability of some of the raw materials needed for LIB devices (e.g., lithium and cobalt) and to their confined geographical distribution [16] still hamper a truly widespread and reliable use of such systems, thus not allowing the growing global market demand to be fulfilled in terms of both battery production throughput and risk for supply shortage or price volatility [17–19].

In this scenario, secondary rechargeable batteries based on sodium, magnesium, aluminum, or potassium ions are garnering attention as greener post-lithium technologies due to the larger abundance and natural availability of their main raw materials [12, 17, 20, 21]. Among them, potassium ion batteries (KIBs) show some potential interesting advantages that make them particularly appealing for stationary applications, domestic use, or load-leveling operations [22]. In particular, in KIBs aluminum can be used as a current collector instead of copper (as in the case of LIBs), since potassium does not form metal alloys with aluminum, unlike lithium. This entails a potential reduction in battery costs and weight. In addition, potassium can provide higher working voltages than other metal-based batteries thanks to its redox potential (−2.93 V vs. standard hydrogen electrode [SHE]), which is similar to the one of Li^+/Li (−3.04 V vs. SHE), but more negative than Na^+/Na (−2.71 V vs. SHE), Mg^{2+}/Mg (−2.37 V vs. SHE), and Al^{3+}/Al (−1.66 V vs. SHE) [21, 23]. Finally, despite the larger ionic radius of K^+, potassium ions can be hosted by commercial graphite anodes typically used in LIBs, as opposed to the sister sodium-based technology. Indeed, they are characterized by a smaller solvated radius and lower desolvation energy, ultimately leading to faster diffusion in the electrolyte and through the electrolyte/electrode interface than what is experienced in lithium and sodium technologies [24–26]. KIB battery technology relies on the "rocking chair" diffusive mechanism of K^+ ions between electrodes via intercalation and deintercalation during the charge/discharge cycles. In the past few years, different potassium hosting materials have been explored as potential cathode (Prussian blue analogs, layered oxides, polyanionic and organic compounds) and anode (carbonaceous, alloying, conversion, and intercalations materials) systems [22]. Due to their high theoretical capacity, potassium metal and alloying materials are considered as interesting anodes for high-energy KIB applications. However, potassium metal can lead to the rupture of the solid electrolyte interphase (SEI) by dendrite formation due to its high reactivity, while alloying materials may undergo non-negligible volume expansions during operation. For these reasons, alternative strategies have also been introduced, based on artificial SEIs, composite nano-sized structures, and electrolyte engineering (salts, additives, polymers, etc...) [22, 27, 28].

A crucial component in KIBs is the electrolyte, which must solubilize the metal ion and provide electrical continuity through ion conduction between the two electrodes. In this context, liquid electrolytes, especially those based on organic carbonates (viz., propylene carbonate [PC], ethylene carbonate [EC], dimethyl carbonate [DMC], diethyl carbonate [DEC]) as solvents in combination with KBF_4, KPF_6, KFSI, KTFSI potassium salts, are widely used in KIBs as they can guarantee high ionic conductivity and effective metal-ion solvation [22, 28]. However, liquid electrolytes are flammable, very volatile, and do not hinder dendrite formation [29, 30] during operation. These negative features represent critical obstacles to safety and battery functionality because they can yield liquid electrolyte leakage and possible thermal runaway (even explosion) due to short circuits resulting from dendrite growth [31, 32]. One approach to overcome these issues relies on the use of gel-polymer electrolytes (GPEs), in which a solid crosslinked polymer network is used to confine the liquid electrolyte and to provide a mechanically stable contact with the electrodes, hindering volumetric expansion and dendrite growth [33, 34]. In this way, increased battery safety and prolonged operational stability can be achieved, without limiting ionic conductivity and device performance as often found in fully solid-state electrolyte systems. While many examples of GPEs for more consolidated battery technologies such as LIBs have appeared in the literature in the past decade [35–38], their development and use in KIBs is still in its infancy. Interestingly, the challenge of controlling and reproducing the thickness of GPEs, which is typically a critical issue in LIBs applications, becomes less significant in KIBs. In particular, in LIBs applications, producing a very thin GPE is crucial for ensuring a high power density to the battery, even at the expense of mechanical strength. Conversely, due to the higher diffusion rate of K-ions across the electrolyte, the trade-off between the mechanical strength of GPEs and the ion diffusion rate is less critical in KIBs compared to their lithium-ion counterparts. This confers to GPEs high potential in KIB technology, as they can provide sufficient ion diffusion while offering enhanced mechanical robustness, ultimately contributing to a longer battery lifespan.

Most GPEs for KIBs are typically obtained from fossil-based polymers, such as poly(methyl methacrylate), poly(ethylene

oxide), and poly(acrylonitrile) [39–41]. In particular, poly (ethylene oxide) is widely used in GPEs and solid-state polymer electrolytes due to the high solvation and high ionic conductivity of the ethylene oxide/ether group with alkaline cations. In this framework, different chemical derivatization strategies of poly(ethylene oxide) have been proposed in the literature via free radical polymerization, atom transfer radical polymerization, reversible addition-fragmentation chain transfer polymerization, or ring-opening polymerization (ROP). More specifically, cyclic ether monomers based on the glycidyl ether moiety have been widely employed in the preparation of polymer electrolytes based on poly(ethylene oxide) through ROP, as this synthetic strategy does not lead to the release of small by-product molecules, retaining the original number of equivalents of monomeric functional groups in the final product [42–44].

On the contrary, very little has been done in the area of bioderived GPEs for KIBs, despite their obvious advantages in terms of renewability and lower carbon footprint compared to their oil-based counterpart [45]. Among the vast array of biobased polymers with suitable characteristics [46–49], lignin represents a particularly interesting material platform for this purpose because it is widely available, highly functional, and highly thermally and mechanically stable [50]. Indeed, lignin has been successfully used as macromolecular precursor for high-value polymeric materials in a variety of engineering and electrochemical applications, including phenolic resins for adhesives, electrodes in energy storage, filler for composite materials, and coatings [51–55]. In particular, a recent work from our groups demonstrated the use of lignin as precursor for the development of a stable GPE yielding excellent operational stability and electrochemical response in KIB devices [56].

Despite the promising performance of this and very few other proposed biobased systems in the KIBs field [51, 57], a detailed description of the relationships between macromolecular structure, materials property, and electrochemical device performance of sustainable GPEs for KIBs is still lacking, despite its strategic importance to enable a rational design of such key element in the battery stack for optimal device performance.

To bridge this gap, in this work, a series of GPEs was prepared using lignin as the base component and poly(ethylene glycol) diglycidyl ether (PEGDGE) as a functional linker. By systematically varying PEGDGE chain length (viz., molecular weight) at constant lignin relative content, detailed structure–property correlations could be highlighted based on an extensive chemical, thermal, mechanical, viscoelastic, and functional characterization of the obtained lignin-based crosslinked membranes. Upon their suitable activation by absorption of liquid electrolyte embedding potassium salts, the influence of PEGDGE chain length on the performance of the resulting GPEs was also elucidated by electrochemical analysis in KIB prototypes.

2 | Results and Discussion

2.1 | KOx-PEGDGE Membranes Characterization

The biobased membranes investigated in this work were obtained by ring-opening polyaddition crosslinking reaction between Fenton pre-oxidized Kraft lignin (KOx) [58–60] and PEGDGE of different molecular weights, namely, 200, 500, and 1000 g mol^{-1} (Figure 1). The reaction was conducted in alkaline water to dissolve lignin and activate its carboxylic, aliphatic, and aromatic OH groups, the latter being particularly reactive according to the literature [61, 62]. The crosslinking process is assumed to proceed via nucleophilic attack of the $-CH_2$ group in the oxirane ring in PEGDGE by the OH groups in KOx [42]. This regioselective nucleophilic attack is favored by the easy accessibility and stabilization effect of the less hindered and substituted carbon atom in the epoxy ring, leading to the formation of a secondary alcohol in the −CH epoxy position [63].

To exclude possible effects of the presence of different residual chemical functionalities on the properties of the resulting crosslinked materials and on the electrochemical performance of the corresponding KIB devices, the molar ratio between epoxy groups in PEGDGE and hydroxyl groups in KOx (quantified through ^{31}P-nuclear magnetic resonance (NMR) spectroscopy, Supporting Information S1: Table S1) was maintained constant at 1.28 $mmol_{epoxy}/mmol_{OHtot\text{-}KOx}$, corresponding to a constant molar-to-mass ratio between PEGDGE and lignin of 4.69 $mmol_{PEGDGE}/g_{KOx}$ for all formulations. This allowed to uniquely identify the contribution given by the chain length of the PEG-based macromolecular linker to the chemical−physical and morphological response of the obtained membranes. Furthermore, the role of PEGDGE in the functional performance of the operating KIB devices could also be assessed, considering the ability of the ethylene-oxide moiety (CH_2–CH_2–O–) to ease ion-pair dissociation into free ions and lead to enhanced ionic conductivity by ion hopping [64–67].

Successful crosslinking reaction between lignin and PEGDGE was confirmed experimentally by gel content analysis, which underlined an insoluble fraction higher than 94% for all membrane formulations (see Supporting Information S1: Table S2). This evidence was further visually corroborated, as mechanically intact and self-supporting membranes could be obtained after the reaction.

2.1.1 | Fourier-Transform Infrared (FTIR) Spectroscopy Analysis

FTIR spectroscopy (Figure 2) was used to investigate the chemical modifications occurring to the reactive species during the crosslinking process and to confirm the successful covalent bonding between PEGDGE and KOx. The FTIR spectra of all the membranes underlined a broad absorption band in the 3650–3200 cm^{-1} range, attributed to the stretching vibration of hydroxyl groups: aliphatic and aromatic −OH, predominantly associated with KOx (Supporting Information S1: Table S1), and secondary alcohol groups formed as a result of the epoxy ring-opening crosslinking reaction with PEGDGE (Figure 1). The increasingly higher intensity and sharpness of the signal in the 3600–3200 cm^{-1} range for membranes incorporating longer PEGDGE linkers may be associated with intramolecular and intermolecular hydrogen-bonded −OH vibrations resulting from the presence of trapped moisture, as the hygroscopic character of the membranes increases [68, 69].

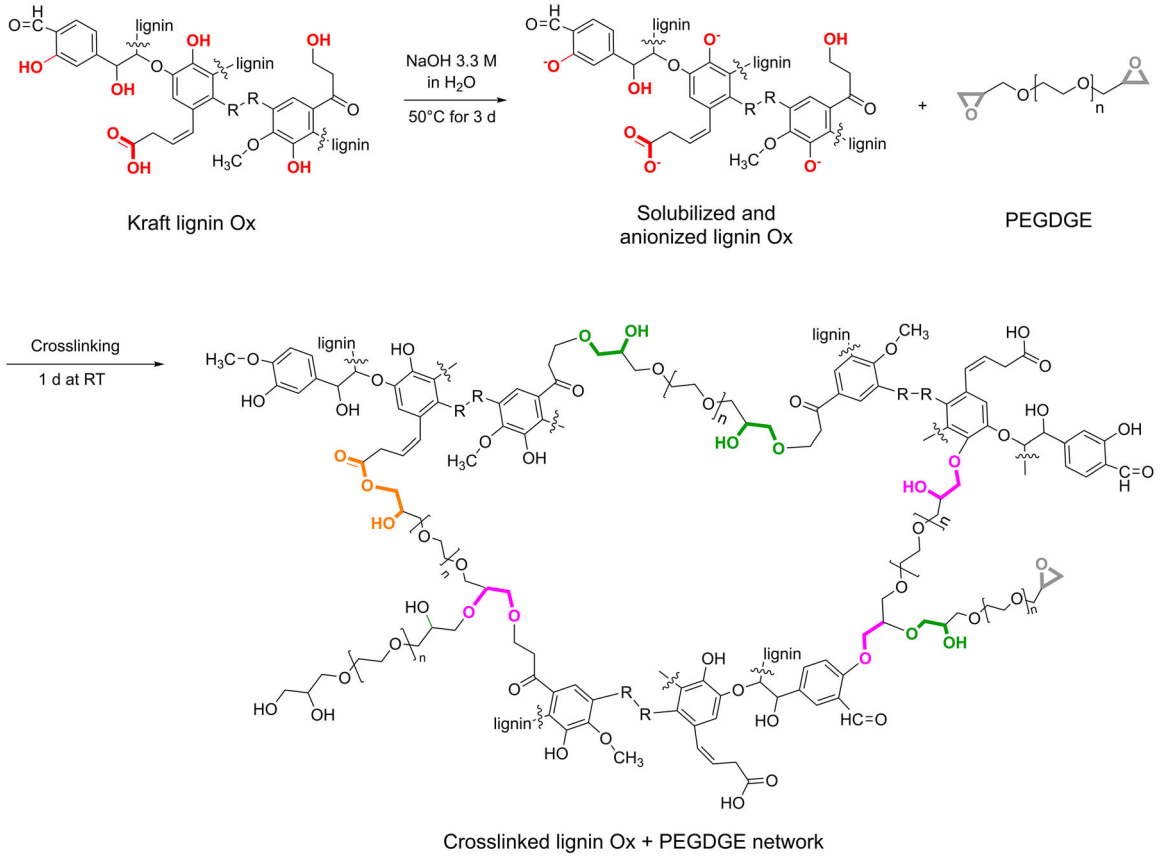

FIGURE 1 | Possible reaction steps associated with the formation of the KOx-PEGDGE membranes. The expected chemical bonds and functional groups formed as a result of the epoxy ring-opening reaction are represented in different colors: aromatic ethers (purple), aliphatic ethers (green), and esters (orange). The obtained crosslinked membranes will be referred to as KOxP, followed by the molecular weight of the used PEGDGE to fabricate them (e.g., the membrane incorporating 1000 g mol^{-1} PEGDGE will be labeled as KOxP1000).

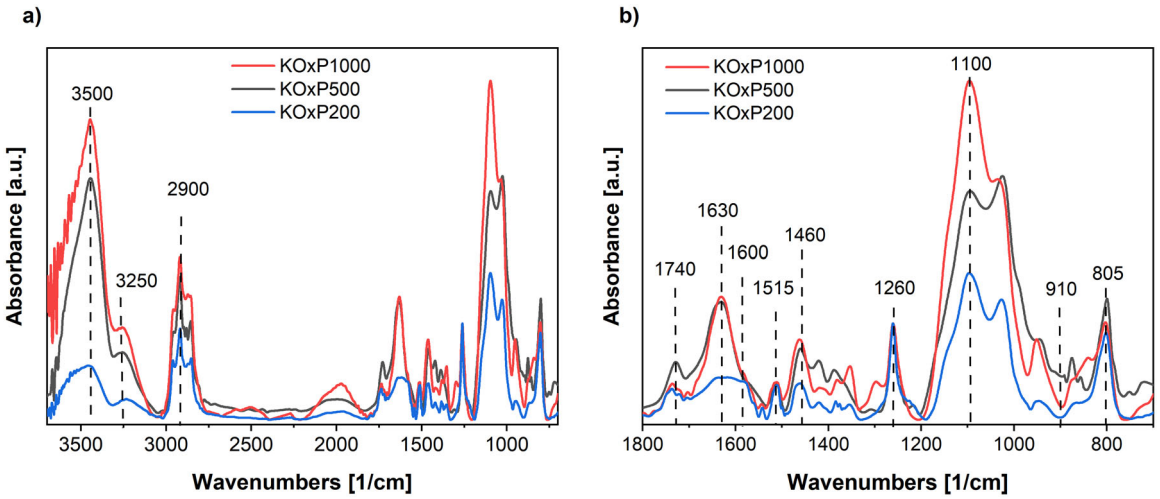

FIGURE 2 | (a) FTIR spectra of KOxP membranes and (b) zoomed fingerprint region. All signals are normalized with respect to the absorbance at 1515 cm^{-1} associated with the invariant aromatic skeletal vibration signal in lignin.

Successful incorporation of PEGDGE was confirmed by the increase in the intensity of the signals in the region 2950–2850 cm^{-1} (C–H stretching vibrations), at 1460 cm^{-1} (asymmetric C–H deformation), and at 1110 cm^{-1} (asymmetric stretching of C–O–C ether bonds in the CH_2–O–CH_2 PEGDGE backbone) for membranes with increasing PEGDGE molecular weight. In addition, effective epoxy ring-opening reaction could be demonstrated by the disappearance of the peak in the 920–880 cm^{-1} region, typically attributable to the asymmetric vibration of the monosubstituted epoxy ring in PEGDGE (Supporting Information S1: Figure S1). Signals associated with C═O stretching vibrations of ketones, carbonyl, and ester

groups in KOx were found at 1740–1700 cm^{-1} (nonconjugated) and 1660–1610 cm^{-1} (conjugated) [70, 71]. In addition, peaks attributable to aromatic skeletal stretching vibrations in lignin were detected at 1600, 1515, and 1420 cm^{-1}, while the signal at 1463 cm^{-1} was ascribed to the combination of aromatic ring vibration with C–H deformation [72]. The sharp absorption band found at 1260 cm^{-1} in all formulations can be related to C–O vibrations in guaiacyl (G) moieties combined with C=O and C–C stretching (the presence of G-units was confirmed by ^{31}P-NMR, see Supporting Information S1: Table S1) [73, 74].

2.1.2 | Thermal Characterization

Differential scanning calorimetry (DSC) was performed to assess the thermal transitions in the oxidized lignin-PEGDGE membranes (Figure 3a). KOxP200 showed a single glass transition (Tg) occurring at 80°C, which was found to be the highest among the different investigated systems. By increasing the molecular weight of PEGDGE in the formulation, a decrease in Tg was observed down to −40°C. This behavior can be associated with the role of the macromolecular PEG chains in PEGDGE, acting as flexible segments in the three-dimensional polymeric network, thereby yielding larger free volume and increased mechanical flexibility of the membrane. Interestingly, while for both KOxP200 and KOxP500 no melting transitions

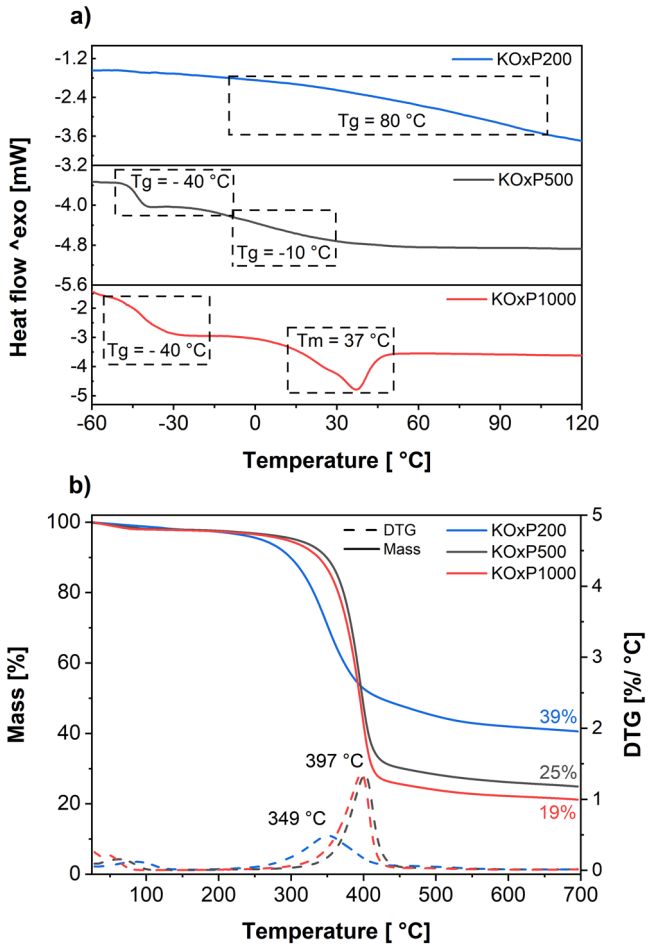

FIGURE 3 | (a) DSC and (b) TGA traces of KOx-PEGDGE based membranes.

(T_m) attributed to the presence of crystalline phases could be detected, a broad endothermic signal peaking at $T_m = 37°C$ was found in KOxP1000. The presence of such melting transition (with lower enthalpy and T_m than the pristine PEGDGE 1000 linker, see Supporting Information S1: Figure S2) could be explained considering the possible crystallization of a fraction of long PEGDGE macromolecular chains due to self-polymerization within the three-dimensional network, as lateral pendant groups or in between crosslinking points (Supporting Information S1: Figure S5) [42, 44, 75–77]. The self-polymerization of PEGDGE likely explains the Tg observed at −40°C in KOxP500, which is similar to the Tg of KOxP1000. This similarity suggests the presence of second-order transitions of long self-polymerized macromolecular chains within the material. However, no crystalline domains (viz., melting transitions) were observed in KOxP500, likely due to the insufficient chain length of PEGDGE 500, as opposed to the longer PEGDGE 1000 in KOxP1000.

The thermolytic stability of lignin-PEGDGE based membranes was evaluated by thermogravimetric analysis (TGA) in N_2 inert atmosphere (Figure 3b). All the three formulations showed less than 1.5% mass loss up to 90°C–100°C, which may be related to the release of trapped moisture associated with the intrinsic hygroscopicity of the membranes. In this temperature range, first-order derivative (DTG) revealed a slightly faster water elimination as the molecular weight of PEGDGE increased. This is likely to be associated with the increased molecular mobility found in membranes incorporating higher molecular weight PEGDGE, in addition to an increased porosity (as will be discussed later on). At higher temperatures, KOxP200 showed excellent thermal stability up to 240°C with a maximum degradation rate at 349°C ($T_{max} = 349°C$), while both KOxP500 and KOxP1000 were found to be stable up to 290°C with a very similar $T_{max} = 397°C$. The single-step thermal decomposition of membranes can be mainly related to the degradation of PEGDGE backbone [33] and of α-β-aryl-alkyl ether linkages and C–C aliphatic chains present in lignin-based membranes after the crosslinking reaction [78]. Interestingly, higher residual mass at 700°C was found for membranes based on lower molecular weight PEGDGE, likely due to the incorporation of higher relative amount of KOx lignin on a mass basis (as corroborated by Table 1 and the TGA thermograms of pristine KOx and PEGDGEs found in Supporting Information S1: Figure S6). This evidence highlights the beneficial effects of the presence of lignin in increasing the high-temperature thermal stability of the membranes upon crosslinking.

2.1.3 | Membrane Morphology and Swelling

The top-surface and cross-section morphology of the obtained membranes after the crosslinking process was investigated by scanning electron microscopy (SEM) on cryo-fractured samples. SEM images (Supporting Information S1: Figure S7) revealed a similar porous membrane morphology for all formulations, with an increasing amount and larger pore dimension found for membranes incorporating higher-molecular-weight PEGDGE. As shown in the SEM images and pore size distribution curves (Supporting Information S1: Figures S7 and S8, respectively), KOxP200 exhibited a very compact structure with finely isolated

TABLE 1 | Formulations and the composition ratio of lignin/PEGDGE-based membranes.

Membrane formulation	Mn PEGDGE (g mol^{-1})	g PEGDGE/g lignin	PEGDGE wt.% in the membrane	Lignin wt.% in the membrane	mmol PEGDGE/g lignin	mmol epoxy/ mmol total OH of KOx
KOxP200	200	0.94	48%	52%		
KOxP500	500	2.34	70%	30%	4.69	1.28
KOxP1000	1000	4.69	83%	17%		

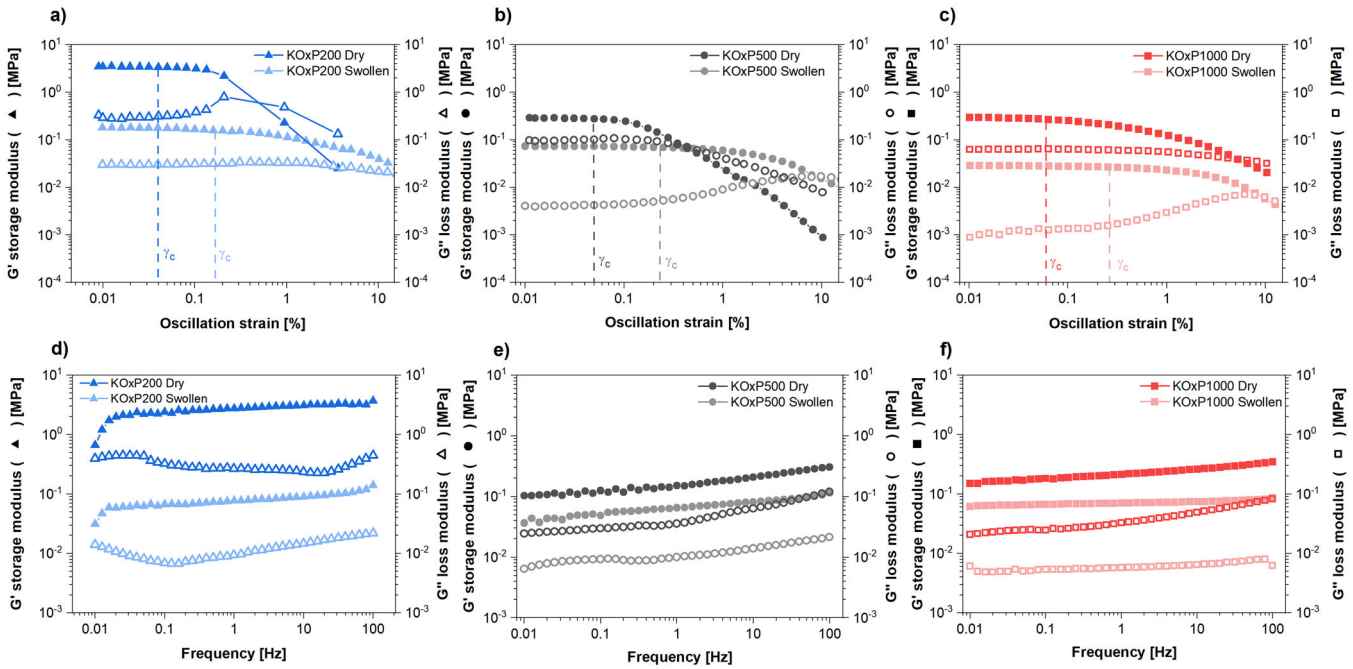

FIGURE 4 | Dynamic rheological results of (a, d) KOxP200, (b, e) KOxP500, and (c, f) KOxP1000. Dynamic strain sweep (a–c); and dynamic frequency sweep analyses (d–f) are reported. In all dynamic strain sweeps, the γ_c is depicted for each system.

pores on the surface ($\varnothing_m \sim 0.75\,\mu m$) and in the inner part of the membrane ($\varnothing_m \sim 0.65\,\mu m$, with few larger, isolated pores of ~8 μm). As opposed to this, a more regular and ordered morphology with larger pore size on the surface ($\varnothing_m \sim 3.1\,\mu m$, and broad pore size distribution) and in the cross-section ($\varnothing_m \sim 1.9\,\mu m$) were found in KOxP500. Finally, KOxP1000 possessed a more irregular morphology characterized by a large number of larger interconnected and interpenetrating pores per unit area both on the surface ($\varnothing_m \sim 3.3\,\mu m$) and in the inner part ($\varnothing_m \sim 2.7\,\mu m$), in line with the polyphasic nature of this material, as evidenced by DSC analysis.

In view of their use as GPEs for KIB devices, the obtained membranes were evaluated in terms of their ability to swell when in contact with an electrolyte medium. To this end, liquid solvent uptake (LSU) measurements were conducted on all membranes in an ethylene carbonate (EC):diethyl carbonate (DEC) 1:1 v/v solution, these latter being supporting solvents commonly employed in KIB systems (Supporting Information S1: Figure S9). In line with the morphological characteristics of the previously discussed membranes, the crosslinked systems incorporating longer-chain PEGDGE (i.e., KOxP500 and KOxP1000) provided larger LSU values, which were found to be compatible with those typically required for GPE application. On the contrary, very modest swelling and insufficient LSU was observed for KOxP200, as a result of its tighter porous structure combined with the lower macromolecular mobility and free volume (i.e., higher Tg) observed on this system, which limits liquid electrolyte penetration and retention in time.

2.1.4 | Mechanical and Viscoelastic Characterization

Together with the extent of membrane swelling in the liquid electrolyte, the viscoelastic response of the material represents another key descriptor of its applicability as GPE for KIBs. To this end, dynamic rheology curves were recorded for the different lignin-based membrane materials monitoring the conservative (G′) and the dissipative (G″) shear moduli at increasing frequency and oscillation-strain amplitude, both in the dry and in the swollen (in EC:DEC 1:1 v/v solution) states (Figure 4). As expected, an approximately one-order of magnitude lower G′ value was observed in swollen membranes versus their dry counterpart irrespective of their composition, as a result of the plasticization effect of the entrapped solvent. Furthermore, the critical oscillation strain (γ_c) defining the extent of the linear viscoelastic region (LVR) (i.e., the region where G′ does not show any dependence on the oscillation strain amplitude) was found to

increase in formulations incorporating PEGDGE of increasingly larger molecular weight ($\gamma_{c\_KOxP200} < \gamma_{c\_KOxP500} < \gamma_{c\_KOxP1000}$, Supporting Information S1: Table S3). This behavior can be correlated with the progressively lower Tg values observed on the different materials (markedly lower for KOxP500 and KOxP1000 than KOxP200), promoting more suitable mechanical resistance and robustness to oscillatory stresses. Accordingly, lower Tg membranes are expected to better accommodate high shear stresses during battery cell assembly and production, thus favoring optimal contact with the electrodes and easier handling during operation.

Interestingly, for all membranes the elastic response (G′) was found to prevail over the viscous response (G″) in the entire frequency domain investigated, further indicating successful and effective crosslinking. This solid-like behavior (G′ > G″) was observed in both dry and swollen states, thus confirming that during the swelling process no dissolution or solvent extraction process takes place on the materials, which could result in disruption of the three-dimensional macromolecular network and decline in mechanical response.

2.2 | Electrochemical Characterization

As evident from the previous discussion, KOxP200 membranes do not appear suitable as GPEs for battery applications because of their dense and compact structure, in addition to their high Tg, extremely low LSU, and unfavorable mechanical response. For these reasons, these systems will not be considered further in this work for electrochemical characterization, which will instead mainly focus on the KOxP1000 formulation compared to KOxP500. Indeed, the presence of larger and interconnected pores in KOxP1000 enables a much higher volume of liquid electrolyte to be incorporated, leading to a record liquid electrolyte uptake > 300% already after 50 min of swelling in potassium hexafluorophosphate (KPF_6) 0.80 M in EC:DEC 1:1 v/v solution (Supporting Information S1: Figure S10).

Activated KOxP1000 membranes were obtained by soaking and swelling these systems in a KPF_6/EC/DEC solution, leading to the target GPE (from here on referred to as GPE1000). To assess their electrochemical performance, half-cells were assembled with potassium foils as anode and current collector, GPE1000 as electrolyte, and carbon black Super P on copper current collector as cathode. Their long-cycling performance was evaluated by testing such half-cells at a constant specific current of 0.05 A g^{-1} for as many cycles as the system could withstand without the occurrence of short circuits and with satisfying retained capacities. Conversely, the half-cell underwent 30 activation cycles before measuring the rate performance, ensuring that the SEI layer was already formed. This approach aimed to exclude the influence of SEI layer formation on performance at increasing current densities. As shown in Figure 5a, after the formation of a stable interface during the first 100 cycles (specific capacity ~130 mAh g^{-1}), long-term

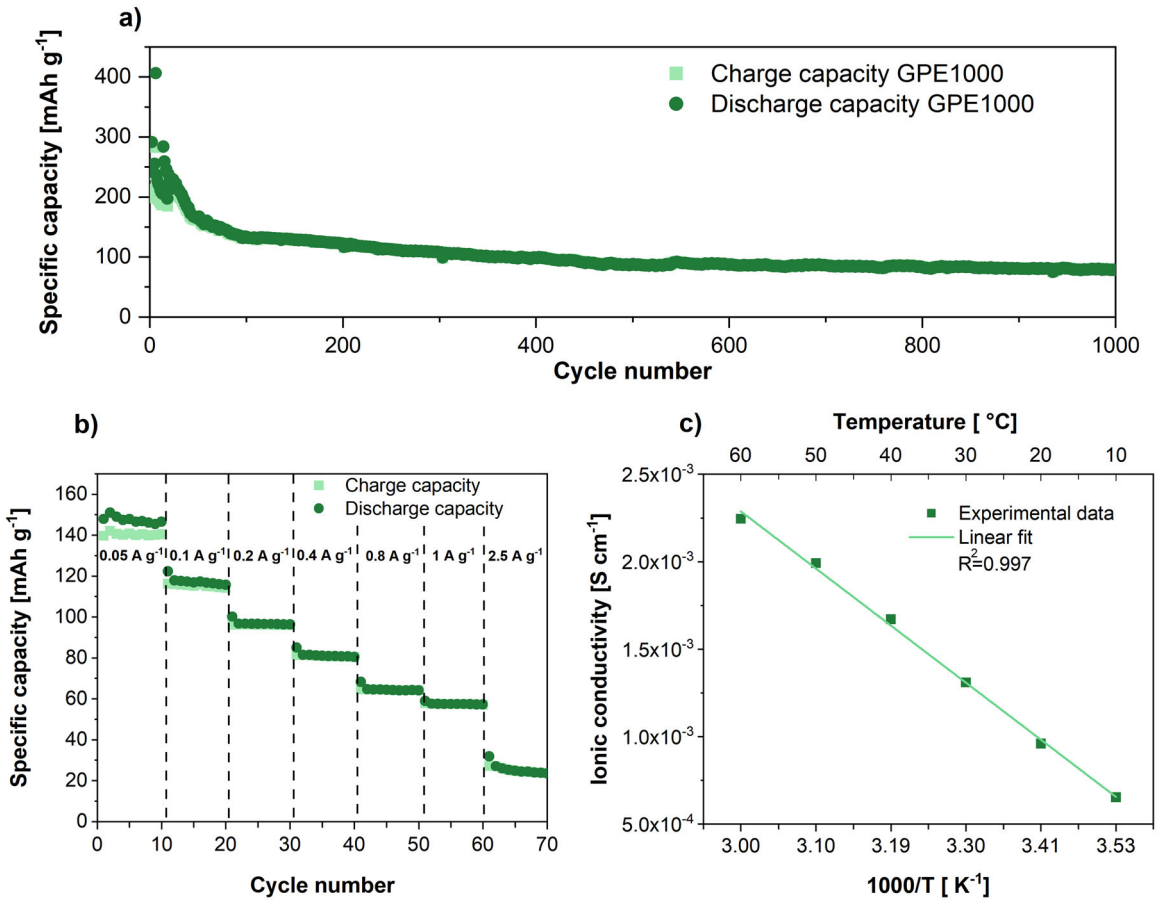

FIGURE 5 | Galvanostatic charge and discharge measurements of K|GPE1000| Super P half cell: (a) long cycling performance at a constant specific current of 0.05 A g^{-1} and (b) current rate performance at different specific currents. (c) Ionic conductivity of GPE1000 at different temperatures.

operation could be attained. After as many as 1000 cycles, the cell could retain 60% of the original capacity shown at the 100th cycle. Notably, continuous stable operation was observed on a much longer cycling time (over 2500 cycles, as shown in Supporting Information S1: Figure S11). To the best of our knowledge, such remarkable stability has never been shown before in the KIBs field. Considering that KIBs based on fossil-derived GPE are scarcely documented, and bio-based GPEs or polymer electrolytes are either unreported or not yet fully investigated electrochemically (e.g., in terms of ionic conductivities with temperature rise, interfacial stability under plating/stripping, and galvanostatic cycling in half-cell or full-cell configurations), the results presented in this work represent a significant milestone in the advancement of sustainable KIB technology (see Supporting Information S1: Table S4). Additionally, from our previous experiences such a high cycling stability in potassium battery cells is also hardly achievable by adopting commercial separators (e.g., Celgard, glass fiber, etc.).

Even superior current rate performance was obtained when comparing K|GPE1000| Super P cells to those based on KOxP500 (Supporting Information S1: Figure S12). Indeed, in contrast with its counterpart, the GPE1000-based system could deliver more stable capacities at each specific current as well as a positive capacity at the highest specific current value of 2.5 A g^{-1} (Figure 5b). Based on these results, additional electrochemical analyses were conducted to better assess the role of longer-chain PEGDGE in such interesting improvement of GPE performance in KIBs. Interestingly, measurements on the ionic conductivity (σ) in symmetrical stainless steel|GPE1000| stainless steel cells at increasing temperatures from 10°C to 60°C (Figure 5c) did not highlight anomalies, as the obtained σ values were found to be in line with those typically reported for fossil-based GPEs in potassium battery application [79–83]. Also, the linear dependence indicates an Arrhenius-like behavior, typical of GPEs in which both the charge transfer in the liquid phase and the ion hopping on the ether groups contribute to the ion conduction. Indeed, both of the ion migration mechanisms have a linear dependence with 1000/T, and it is not possible to distinguish one contribution from the other. Notably, these ionic conductivity values were comparable to or even exceeded those of bio-based potassium-ion-conducting polymer electrolytes and bio-derived GPEs reported in the literature, as summarized in Supporting Information S1: Table S4.

The diversified nonhomogenous morphology of the KOxP1000 membrane, characterized by the presence of randomly alternating ordered and disordered regions (SEM analysis, Supporting Information S1: Figure S7), may also lead to nonuniform ion transfer through the electrode/electrolyte interface, ultimately resulting in nonuniform plating on the potassium metal surface. This potential phenomenon was investigated by means of plating and stripping tests carried out on a symmetrical cell (K|GPE1000|K) at increasing current density values (i.e., 0.1 and 0.5 mA cm^{-2}) for 35 cycles of 2 h each (i.e., 1 h at positive current and 1 h at negative current). The overpotential profile depicted in Figure 6 shows a perfectly symmetrical peaking profile at lower current density, resulting from the superposition of two parallel kinetic pathways, namely, plating on one electrode and stripping on the other one. With the increase of the current density up to 0.5 mA cm^{-2}, some needle-shaped peaks appeared, which are symptoms of possible nucleation and growth of metal dendrites. These may be caused by a nonperfectly uniform and stable solid electrolyte interphase (SEI) layer that can be subjected to cracks with the subsequent formation of pits on the metal surface, especially for more challenging charge transfer. It has been shown that alkali ions tend to nucleate on these pits [84], creating a non-homogeneous surface and inducing a reversible process of plating-on/stripping from mossy dendrites. This behavior is typically represented by arcing voltage profiles, as those found in Figure 6. Since the electrochemical characterization is intended to assess the GPE capacity to work properly and safely even in the most challenging conditions, we intentionally chose not to rely on the use of additives when formulating the electrolyte, the duty of which is to form stable SEI layers to avoid as much as possible unfavorable conditions for the battery operation. With the same purpose, the current density was increased up to 1.5 mA cm^{-2} during the test, a widely recognized very high value for electrolyte characterization. Indeed, at this current density the formation of dendrites is typically encountered, with the consequent collapse of the electrolyte/potassium metal interface, ultimately leading to short-circuit or rectangular-shaped overpotential profiles. The latter is caused by the presence of a very high surface area coming from the large number of dendrites and "death-potassium" resulting from the detachment of the dendrites, which yields a very low applied current per cm^2. Interestingly, as never achieved in the KIB literature before, none of the above mechanisms was observed in our systems. Indeed, no anomalies in the electrochemical impedance spectra or short-circuits were recorded (Supporting Information S1: Figure S13).

2.3 | Correlations Between Material Properties, Electrolyte Structure, and Electrochemical Response

The observed differences in electrochemical performance and material properties discussed in the previous sections are attributed to the synergistic interplay between the composition of the formulations and the morphological and macromolecular structure of KOxP/GPEs systems. The incorporation of PEGDGE with increasing molecular weights (200, 500 and 1000 g mol^{-1}) at constant 1.28 $mmol_{epoxy}/mmol_{OHtot\text{-}Kox}$ ratio resulted in an improvement in thermal and macromolecular properties of the crosslinked KOxP membrane systems. In particular, the thermolytic stability was enhanced, ranging from 240°C for KOxP200 to 397°C for KOxP500 and KOxP1000. Moreover, the incorporation of longer macromolecular PEGDGE chains resulted in higher network mobility, as evidenced by a decrease in Tg for the corresponding membranes, namely, 80°C for KOxP200 and −40°C for KOxP500 and KOxP1000. These results can be associated with larger free volume and molecular mobility due to the presence of longer flexible polymeric bridges between crosslinking points (Mc) in the crosslinked network (the higher the molecular weight of the PEGDGE crosslinker, the longer Mc) [44, 82]. These features are highly desirable in polymer electrolytes for battery applications, since low Tg and low crystalline fraction are known to enhance ionic conductivity [85–87].

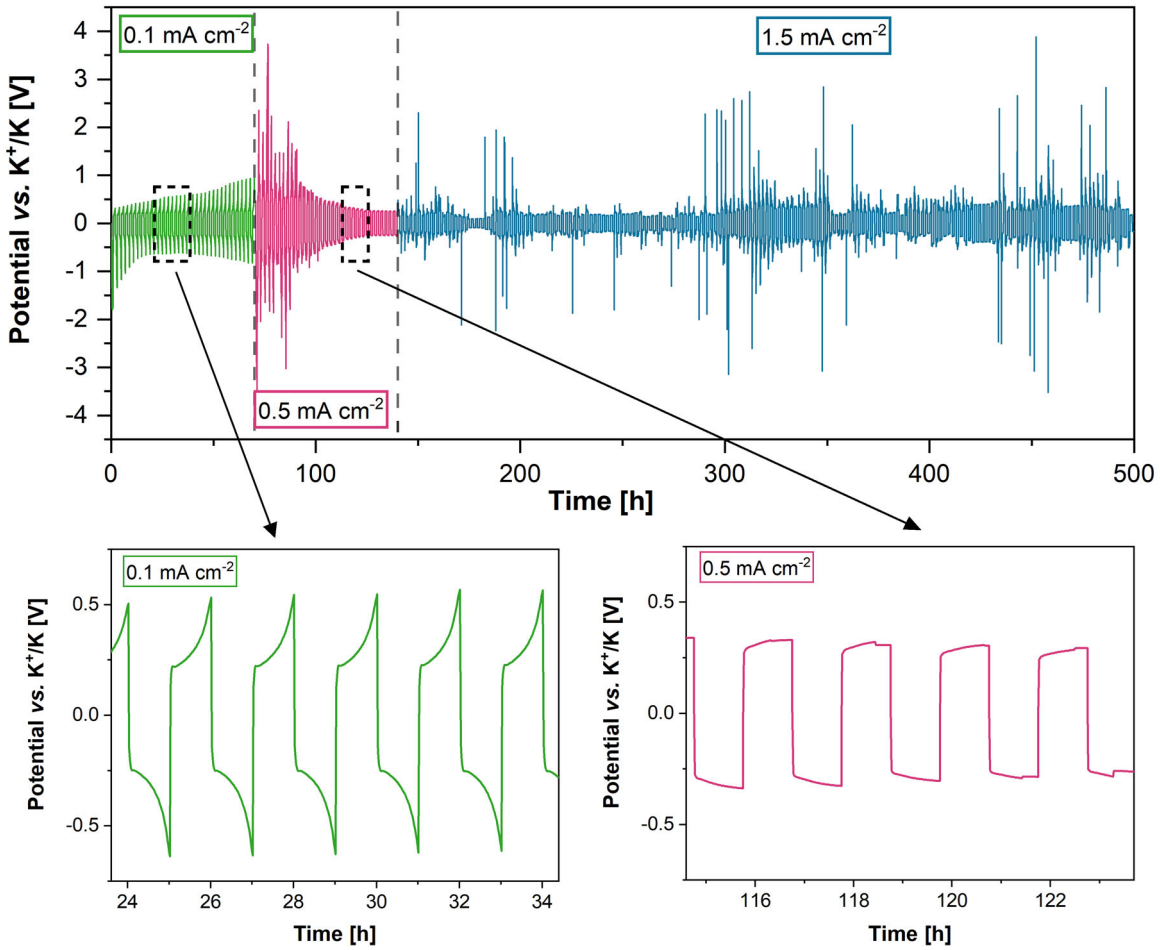

FIGURE 6 | Overpotential profile of the symmetric K|GPE1000|K cell subjected to 500 h of plating and stripping at three increasing current density values (i.e., 0.1, 0.5, and 1.5 mA cm^{-2}). The left inset shows the zoomed peaking symmetrical profile and the right inset highlights the stable arcing behavior.

As shown in Supporting Information S1: Figure S7, the dense and compact structure of KOxP200, with sub-micron pore dimensions (< 1 μm) and high stiffness (Tg = 80°C), limited liquid electrolyte penetration and uptake, highlighting the negative impact of the lowest molecular weight PEGDGE linker (200 g mol^{-1}) on Mc, and consequently on the available free volume. The rigid structure of KOxP200 hinders the uptake of solvent resulting in only 20% of LSU (Supporting Information S1: Figure S9). However, when the potassium salt dissolves in the liquid electrolyte and attempts to penetrate, the chain mobility is so sluggish that the LEU remains zero even after 10 h, making the membrane unsuitable as a polymer electrolyte. Consequently, KOxP200 could not be electrochemically characterized.

In the case of GPE1000 and GPE500, similar values for ionic conductivity σ were obtained (Supporting Information S1: Figure S14). This trend may be explained considering the tradeoff between the higher amount of uptaken solvated potassium salts in solution (i.e., higher number of ionic species contributing to σ; Supporting Information S1: Figure S15) during membrane swelling, and the presence of crystalline phases in GPE1000/KOxP1000 hindering ion mobility (DSC traces in Figure 3), likely resulting from self-polymerization of PEGDGE during the crosslinking reaction.

Interestingly, membranes incorporating the longest PEGDGE chains (GPE1000) resulted in the best battery performance in terms of durability and specific capacity (Supporting Information S1: Figures S11 and S12). We speculate that the ability of our GPEs to withstand such high current densities for so many cycles may be associated with their favorable elastic behavior. Indeed, an extended LVR (γ_c) was observed in membranes incorporating increasingly longer PEGDGE linkers, which was found to be the largest in GPE1000 (Figure 4). This extended linear viscoelastic response over a wide range of mechanical stresses, such as those typically resulting from dendrite formation, is expected to preserve excellent contact with the electrodes during operation, while being enough mechanically robust to suppress further dendrite growth, ultimately ensuring appreciable specific capacities for over 2500 cycles. Moreover, the higher liquid electrolyte incorporation and concentration of solvated potassium salts found in GPE1000 (Supporting Information S1: Figure S15) is also expected to counterbalance the consumption of chemical species taking place during SEI formation in the first cycles of operation and the progressive, slow degradation of KPF_6 and EC:DEC carbonate solvents [88–90], ultimately leading to excellent long-term performance retention during battery lifetime.

3 | Conclusion

A series of lignin-based membranes were successfully synthesized by ring-opening polyaddition crosslinking reaction between pre-oxidized Kraft lignin and PEGDGE of different molecular weights (200, 500, and 1000 g mol^{-1}). To compare these systems, a constant 1.28 $mmol_{epoxy}/mmol_{OHtot\text{-}Kox}$ ratio corresponding to a fixed molar-to-mass ratio between PEGDGE and lignin of 4.69 $mmol_{PEGDGE}/g_{KOx}$ was maintained fixed for all formulations. The influence of PEGDGE chain length on the physico-chemical properties and electrochemical performance of the resulting membranes as GPEs for KIB was investigated. The increase in the molecular weight of PEGDGE was found to slightly increase the thermolytic stability from 240°C for KOxP200 to 397°C for KOxP500 and KOxP1000. This was accompanied by a decrease in the Tg of the membranes, namely, 80°C for KOxP200 and −40°C for KOxP500 and KOxP1000. Second-order transitions were also observed in KOxP500 and a crystalline phase with $T_m = 37$°C in KOxP1000 was visible, likely attributed to self-polymerization of PEGDGE during the crosslinking reaction. However, this residual crystallinity in KOxP1000 did not appear to negatively affect the electrochemical properties of the corresponding membrane. The mechanical properties of the membranes were determined by rheology measurements in dry and swollen states, evidencing a slight decrease of the elastic modulus G′ and an extended LVR (γ_c) for systems incorporating increasingly longer PEGDGE linker. Additionally, an approximately one-order of magnitude lower G′ value was observed in swollen membranes versus their dry counterpart, irrespective of their composition. The crosslinked systems with longer-chain PEGDGE (KOxP500 and KOxP1000) exhibited larger LSU values, suitable for GPE applications. In contrast, KOxP200 showed minimal swelling and insufficient LSU due to its tighter porous structure and lower macromolecular mobility (i.e., higher Tg), which hindered liquid electrolyte penetration and soaking. For these reasons, only KOxP500 and KOxP1000 were found to be viable for testing as GPEs after activation by means of a liquid electrolyte embedding potassium salts.

Accordingly, GPE500 and GPE1000 were investigated in potassium metal cell prototypes, exhibiting an ionic conductivity of ~10^{-3} S cm^{-3} at ambient temperature, on par with those reported in the literature in the GPE field for potassium-based batteries. Interestingly, systems incorporating GPE based on PEGDGE 1000 g mol^{-1} could reach specific capacities as high as 130 mAh g^{-1} at 0.05 A g^{-1} in the first 100 cycles and long-term durability of over 2500 cycles, representing outstanding achievements as bio-sourced systems for potassium batteries. Moreover, GPE1000-based devices were shown to tolerate current densities as high as 1.5 mA cm^{-2}, validating the ability of this membrane formulation to withstand dendrites over long cycles without leading to short circuits.

This work provides the first detailed description of the relationships between macromolecular structure, materials property, and electrochemical device performance of sustainable GPEs for KIBs, paving the path for the definition of design guidelines for the development of future high-performance biobased GPEs for stable and sustainable KIB devices.

4 | Experimental Section

4.1 | Materials

The kraft lignin (Indulin AT) used in this project was supplied by Ingevity. Poly(ethylene glycol) diglycidyl ether (PEGDGE 200, Mn ~200 g mol^{-1}) and poly(ethylene glycol) diglycidyl ether (PEGDGE 1000, Mn ~1000 g mol^{-1}) were purchased from Polysciences. Poly (ethylene glycol) diglycidyl ether (PEGDGE 500, Mn ~500 g mol^{-1}), ferrous chloride tetrahydrate ($FeCl_2 \cdot 4H_2O$, analytical grade), hydrogen peroxide (H_2O_2, 30 wt% in H_2O), sulfuric acid (H_2SO_4, ACS reagent, 95%−98%), sodium hydroxide (NaOH, EMSURE ACS, Reag. Ph Eur, ISO, pellets), tetrahydrofuran (THF, contains BHT as inhibitor, ACS reagent, ≥ 99.0%), diethyl carbonate (DEC, 99%), and ethylene carbonate (EC, 98%) were provided by Sigma-Aldrich. All the mentioned chemicals were used without any further purification before their use. Potassium (cubes in mineral oil, 99.5% trace metals basis), potassium hexafluorophosphate (KPF_6, 99.5% trace metals basis), and *N*-methyl-2-pyrrolidone were provided by Merck. Battery grade EC and DEC were bought from Solvionic. Carbon black Super-P and poly(vinylidene fluoride) were purchased from Alfa Aesar.

4.2 | Membrane Fabrication

4.2.1 | Lignin Oxidation

Pristine lignin was pre-functionalized via Fenton oxidation reaction to obtain oxidized Kraft lignin (KOx). This preliminary step was required to increase the amount and the reactivity of OH groups involved in the epoxy ring-opening crosslinking reaction with PEGDGE to obtain a stable and self-standing membrane, as reported in the literature [58–60]. Briefly, lignin (25 wt%; 0.25 g_{lignin}/ml_{H_2O}) was dispersed in deionized water and left under stirring for 30 min in a conical flask. $FeCl_2 \cdot 4H_2O$ (0.025 $mmol/g_{lignin}$) was added to the suspension and stirred for additional 30 min. H_2O_2 was added dropwise to achieve a concentration of 0.3% $V_{H_2O_2}/V_{H_2O}$ in the reaction mixture. After 24 h of continuous stirring at room temperature in a conical flask, the mixture was air-dried in a Petri dish at room temperature. KOx in the form of a brownish powder was finally obtained after drying overnight in vacuum oven at 50°C.

4.2.2 | KOx-PEGDGE Crosslinking

The crosslinking step was carried out using a modified procedure compared with those reported in the literature [56, 60, 62, 91], KOx (25 wt%; 0.25 g_{KOx}/ml_{H_2O}) was dissolved in a NaOH 3.3 M aqueous solution under stirring at 50°C for 3 days in a parafilm-capped glass beaker to prevent water evaporation. Then, the solution was cooled down to room temperature while keeping it under stirring for the subsequent addition of PEGDGE, according to the aggregation state of this difunctional linker: liquid PEGDGE 200 and PEGDGE 500 were poured into the solution, instead PEGDGE 1000 (solid/waxy) was previously melted in a beaker at 40°C and then quickly added to the solution. After 1 min of stirring, then the KOx-PEGDGE formulation was deposited on a glass Petri dish covered on the surface with a cellulose acetate film to facilitate membrane detachment once

consolidated. The deposited formulation was left to crosslink for 1 day at room temperature under a fume hood. The resulting alkaline membranes were rinsed thoroughly with plenty of deionized water and neutralized with H_2SO_4 0.05 M dropwise until a neutral pH was reached. The neutralized membranes were finally air-dried on poly(tetrafluoroethylene) substrates and then dried overnight in vacuum oven at 50°C (the composition of the prepared formulations is reported in Table 1). The obtained crosslinked membranes will be referred to as KOxP, followed by the molecular weight of the used PEGDGE to fabricate them.

4.3 | Gel Content (GC) Measurements

GC analyses were performed by immersing a ~50 mg vacuum-dried membrane sample in 20 mL of THF, which is proved to be a good solvent both for lignin [92] and PEGDGE. After 24 h of stirring at 40°C, the sample was extracted and completely dried in a vacuum oven. The gel (insoluble) fraction was determined gravimetrically following Equation (1), where m_0 and m_f refer to the dry mass of the initial and final sample after the GC analysis, respectively.

$$\mathrm{GC} = \frac{m_f}{m_0} \cdot 100. \quad (1)$$

4.4 | Fourier-Transform Infrared (FTIR) Spectroscopy

FTIR spectroscopy was conducted on a Nicolet 760 FTIR spectrophotometer. The membrane sample was previously dried in vacuum oven overnight at 50°C, then it was crushed and reduced to powder in a mortar after being immersed in liquid nitrogen. The powder was dried in vacuum oven overnight at 50°C and then compounded with KBr powder to obtain a circular disk with the use of a hydraulic press.

FTIR spectra were acquired using 64 cumulative scans with a resolution of 4 cm^{-1} in a wavenumber range of 4000–400 cm^{-1} in transmission mode in air at ambient temperature.

4.5 | Thermogravimetric Analysis (TGA)

TGA was carried out on KOxP membranes by using a TA Thermogravimetric Analyzer TGA Q500. The analysis was conducted on approximately 10 mg samples by applying a heating rate of 10°C min^{-1} under nitrogen inert atmosphere from 25°C to 700°C. The degradation onset temperature, the temperature at maximum degradation rate, the sample residual mass, the mass loss, and the mass loss derivative (first-order thermal derivative) curves were recorded and assessed.

4.6 | DSC

DSC was employed to evaluate glass transition temperature (Tg), and melting temperature of crystalline phases related to lignin/PEGDGE-based membranes. The analysis was performed using a Mettler Toledo DSC/823e instrument on approximately 10 mg samples placed in a hermetically sealed aluminum pan. Three thermal scans were carried out, specifically heating/cooling/heating from −80°C to 200°C at 20°C min^{-1} heating rate. In the second heating ramp, Tg was assessed as the inflection point of the recorded heat flow curve.

4.7 | SEM

SEM analyses were performed on the surface and cryo-fractured cross-section of the sample using a Carl Zeiss EVO 50 extended pressure scanning electron microscope (acceleration voltage from 15 to 17.5 kV). The pore size distribution and the average pore diameter ($\varnothing_m$) in the prepared membranes were determined by analyzing surface and cross-section SEM images using Image-Pro Plus software. For each log-normal distribution curve, three SEM images were analyzed per sample, measuring the diameters of at least 100 pores.

4.8 | LSU and LEU

LSU and LEU analyses were performed at room temperature to assess the capability of membranes to soak up supporting solvents (EC:DEC 1:1 v/v) and liquid electrolyte solution with potassium ions (KPF_6 0.80 M in EC:DEC 1:1 v/v), respectively. Approximately 50 mg of membrane sample were dried at 50°C the night before and then weighed (m_0). Subsequently, the dried membrane was placed in the liquid electrolyte solution and, after different time intervals (Supporting Information S1: Figures S9, S10, and S15), the mass of the swollen sample was measured by weighing (m_t).

The degree of liquid uptake was calculated according to Equation (2):

$$\mathrm{LSU/LEU} = \frac{m_t - m_0}{m_0} \cdot 100. \quad (2)$$

4.9 | Dynamic Rheology

Dynamic rheology analyses on KOxP membranes were carried out at 25°C in the swollen (in solution EC:DEC 1:1 v/v) and in unswollen dry state by using 20 mm stainless steel parallel plate geometry and a Peltier-plate temperature control installed on a TA Instruments Discovery DHR2 stress-controlled rheometer. The LVR was evaluated between 0.01% and 10% oscillation strain amplitude at a constant frequency of 50 Hz. Frequency sweep analyses were performed in shear mode in the 0.01–100 Hz frequency range at constant 0.03% oscillation strain amplitude to lie within the LVR for each sample type with the same strain amplitude. A constant normal axial force was applied to the specimen throughout the analysis (1 N and 0.5 N for the dry and swollen specimen, respectively) to ensure reliable contact of the material with the rheometer plates. The critical strain for the LVR range (γ_c) was computed in dynamic strain sweep analyses as the value of strain amplitude after which the elastic modulus G′ drops below 95% of its initial plateau value encountered at low strains.

4.10 | Electrochemical Characterization

The crosslinked polymer membranes were activated by swelling in KPF_6 0.8 M in 1:1 EC:DEC standard liquid electrolyte for over 20 h. The activated KOxP polymer membranes are referred to as gel-polymer electrolyte (GPE). All the electrochemical characterizations of GPEs (i.e., ionic conductivity, plating and stripping, and the rate and long cycling performance) were performed in symmetrical or half-cell configurations by using ECC-Std electrochemical cells (EL-CELL GmbH). Electrochemical testing conditions were those commonly adopted in the KIB framework, and the reader can refer to relevant literature for details [51].

Acknowledgments

This study was carried out within the «GREEN2MOVE» project [FISA-2022-00983] funded by Ministero dell'Università e della Ricerca (Bando FISA 2022), and within the Agritech National Research Center funded by the European Union Next-GenerationEU (National Recovery and Resilience Plan (Piano Nazionale di Ripresa e Resilienza - PNRR) – Mission 4 Component 2, Investment Line 1.4 – D.D. 1032 17/06/2022, CN00000022). This research has also received funding from the European Union's Horizon 2020 Research and Innovation Program (grant agreement no. 952941; project: BIOMAC), and from Regione Lombardia ("Collaboration agreement for the creation of an innovative pilot regional infrastructure to support the transition towards the circular economy", project: EcoCIRC Regional Hub).

Conflicts of Interest

The authors declare no conflicts of interest.

Data Availability Statement

The data that support the findings of this study are available from the corresponding author upon reasonable request.

References

1. M. Zhou, P. Bai, X. Ji, J. Yang, C. Wang, and Y. Xu, "Electrolytes and Interphases in Potassium Ion Batteries," *Advanced Materials* 33, no. 7 (2021): 2003741.

2. V. Anoopkumar, B. John, and T. D. Mercy, "Potassium-Ion Batteries: Key to Future Large-Scale Energy Storage?," *ACS Applied Energy Materials* 3, no. 10 (2020): 9478–9492.

3. M. S. Guney and Y. Tepe, "Classification and Assessment of Energy Storage Systems," *Renewable and Sustainable Energy Reviews* 75 (2017): 1187–1197.

4. N. L. Panwar, S. C. Kaushik, and S. Kothari, "Role of Renewable Energy Sources in Environmental Protection: A Review," *Renewable and Sustainable Energy Reviews* 15, no. 3 (2011): 1513–1524.

5. C. Furlan and C. Mortarino, "Forecasting the Impact of Renewable Energies in Competition With Non-Renewable Sources," *Renewable and Sustainable Energy Reviews* 81 (2018): 1879–1886.

6. A. B. Gallo, J. R. Simões-Moreira, H. K. M. Costa, M. M. Santos, and E. Moutinho dos Santos, "Energy Storage in the Energy Transition Context: A Technology Review," *Renewable and Sustainable Energy Reviews* 65 (2016): 800–822.

7. W. F. Pickard, A. Q. Shen, and N. J. Hansing, "Parking the Power: Strategies and Physical Limitations for Bulk Energy Storage in Supply–Demand Matching on a Grid Whose Input Power Is Provided by Intermittent Sources," *Renewable and Sustainable Energy Reviews* 13, no. 8 (2009): 1934–1945.

8. B. Kale and S. Chatterjee, "Electrochemical Energy Storage Systems: India Perspective," *Bulletin of Materials Science* 43, no. 1 (2020): 96.

9. Y. Sun, Z. Zhao, M. Yang, D. Jia, W. Pei, and B. Xu, "Overview of Energy Storage in Renewable Energy Power Fluctuation Mitigation," *CSEE Journal of Power and Energy Systems* 6, no. 1 (2020): 160–173.

10. G. Coppez, S. Chowdhury, and S. P. Chowdhury, "The Importance of Energy Storage in Renewable Power Generation: A Review," In *45th International Universities Power Engineering Conference UPEC 2010*, (United Kingdom: Institute of Electrical and Electronics Engineers [IEEE], 2010), 1281–1285.

11. H. Kim, J. Hong, K. Y. Park, H. Kim, S. W. Kim, and K. Kang, "Aqueous Rechargeable Li and Na Ion Batteries," *Chemical Reviews* 114, no. 23 (2014): 11788–11827.

12. T. Placke, R. Kloepsch, S. Dühnen, and M. Winter, "Lithium Ion, Lithium Metal, and Alternative Rechargeable Battery Technologies: The Odyssey for High Energy Density," *Journal of Solid State Electrochemistry* 21, no. 7 (2017): 1939–1964.

13. B. Wang, W. Du, Y. Yang, et al., "Two-Dimensional Germanium Sulfide Nanosheets as an Ultra-Stable and High Capacity Anode for Lithium Ion Batteries," *Chemistry—A European Journal* 26, no. 29 (2020): 6554–6560.

14. Y. Zhao, O. Pohl, A. I. Bhatt, et al., "A Review on Battery Market Trends, Second-Life Reuse, and Recycling," *Sustainable Chemistry* 2, no. 1 (2021): 167–205.

15. J. M. Tarascon and M. Armand, "Issues and Challenges Facing Rechargeable Lithium Batteries," *Nature* 414 (2001): 359–367.

16. B. K. Sovacool, S. H. Ali, M. Bazilian, et al., "Sustainable Minerals and Metals for a Low-Carbon Future," *Science* 367, no. 6473 (2020): 30–33.

17. C. Vaalma, D. Buchholz, M. Weil, and S. Passerini, "A Cost and Resource Analysis of Sodium-Ion Batteries," *Nature Reviews Materials* 3, no. 4 (2018): 18013.

18. European Commission, *Communication From the Commission to the European Parliament, the Council, the European Economic and Social Committee and the Committee of the Regions Youth Opportunities Initiative* (European Commission, 2011).

19. Inkwood Research, *Size of the Global Battery Market From 2018 to 2021, With a Forecast Through 2030, by Technology (in Million U.S. dollars)* 2022, https://www.statista.com/statistics/1339880/global-battery-market-size-by-technology/.

20. Statista Estimates; BloombergNEF; US Department of Energy, *Projected Global Battery Demand From 2020 to 2030, by Application (in Gigawatt Hours)* 2021, https://www.statista.com/statistics/1103218/global-battery-demand-forecast/.

21. M. Walter, M. V. Kovalenko, and K. V. Kravchyk, "Challenges and Benefits of Post-Lithium-Ion Batteries," *New Journal of Chemistry* 44, no. 5 (2020): 1677–1683.

22. R. Rajagopalan, Y. Tang, X. Ji, C. Jia, and H. Wang, "Advancements and Challenges in Potassium Ion Batteries: A Comprehensive Review," *Advanced Functional Materials* 30, no. 12 (2020): 1909486.

23. Y. Xu, T. Ding, D. Sun, X. Ji, and X. Zhou, "Recent Advances in Electrolytes for Potassium-Ion Batteries," *Advanced Functional Materials* 33, no. 6 (2023): 2211290.

24. Q. Yao and C. Zhu, "Advanced Post-Potassium-Ion Batteries as Emerging Potassium-Based Alternatives for Energy Storage," *Advanced Functional Materials* 30, no. 49 (2020): 2005209.

25. Z. Zhang, M. Li, Y. Gao, et al., "Fast Potassium Storage in Hierarchical $Ca_{0.5}Ti_2(PO_4)_3$@C Microspheres Enabling High-Performance Potassium-Ion Capacitors," *Advanced Functional Materials* 28, no. 36 (2018): 1802684.

26. K. Lei, F. Li, C. Mu, et al., "High K-Storage Performance Based on the Synergy of Dipotassium Terephthalate and Ether-Based Electrolytes," *Energy & Environmental Science* 10, no. 2 (2017): 552–557.

27. Z. Liu, X. Liu, B. Wang, et al., "Ultra-Thick, Dense Dual-Encapsulated Sb Anode Architecture With Conductively Elastic Networks Promises Potassium-Ion Batteries With High Areal and Volumetric Capacities," *eScience* 3, no. 6 (2023): 100177.

28. L. Ni, G. Xu, C. Li, and G. Cui, "Electrolyte Formulation Strategies for Potassium-Based Batteries," *Exploration* 2, no. 2 (2022): 20210239.

29. Y. K. Liu, C. Z. Zhao, J. Du, X. Q. Zhang, A. B. Chen, and Q. Zhang, "Research Progresses of Liquid Electrolytes in Lithium-Ion Batteries," *Small* 19, no. 8 (2023): 2205315.

30. B. Li, Y. Chao, M. Li, et al., "A Review of Solid Electrolyte Interphase (SEI) and Dendrite Formation in Lithium Batteries," *Electrochemical Energy Reviews* 6, no. 1 (2023): 7.

31. P. Jaumaux, J. Wu, D. Shanmukaraj, et al., "Non-Flammable Liquid and Quasi-Solid Electrolytes Toward Highly-Safe Alkali Metal-Based Batteries," *Advanced Functional Materials* 31, no. 10 (2021): 2008644.

32. N. E. Galushkin, N. N. Yazvinskaya, and D. N. Galushkin, "Mechanism of Thermal Runaway in Lithium-Ion Cells," *Journal of the Electrochemical Society* 165, no. 7 (2018): A1303–A1308.

33. X. Gong, D. Shi, H. Zeng, et al., "Facile One Pot Polycondensation Method to Synthesize the Crosslinked Polyethylene Glycol-Based Copolymer Electrolytes," *Macromolecular Chemistry and Physics* 217, no. 14 (2016): 1607–1613.

34. Y. Wang, J. Qiu, J. Peng, J. Li, and M. Zhai, "One-Step Radiation Synthesis of Gel Polymer Electrolytes With High Ionic Conductivity for Lithium-Ion Batteries," *Journal of Materials Chemistry A* 5, no. 24 (2017): 12393–12399.

35. X. Cheng, J. Pan, Y. Zhao, M. Liao, and H. Peng, "Gel Polymer Electrolytes for Electrochemical Energy Storage," *Advanced Energy Materials* 8, no. 7 (2018): 1702184.

36. W. Ren, C. Ding, X. Fu, and Y. Huang, "Advanced Gel Polymer Electrolytes for Safe and Durable Lithium Metal Batteries: Challenges, Strategies, and Perspectives," *Energy Storage Materials* 34 (2021): 515–535.

37. J. Pan, N. Wang, and H. J. Fan, "Gel Polymer Electrolytes Design for Na-Ion Batteries," *Small Methods* 6, no. 11 (2022): 2201032.

38. S. Liang, W. Yan, X. Wu, et al., "Gel Polymer Electrolytes for Lithium Ion Batteries: Fabrication, Characterization and Performance," *Solid State Ionics* 318 (2018): 2–18.

39. Z. Xiao, B. Zhou, J. Wang, et al., "PEO-Based Electrolytes Blended With Star Polymers With Precisely Imprinted Polymeric Pseudo-Crown Ether Cavities for Alkali Metal Ion Batteries," *Journal of Membrane Science* 576 (2019): 182–189.

40. N. K. Jyothi, K. K. Venkataratnam, P. N. Murty, and K. V. Kumar, "Preparation and Characterization of PAN–KI Complexed Gel Polymer Electrolytes for Solid-State Battery Applications," *Bulletin of Materials Science* 39, no. 4 (2016): 1047–1055.

41. H. Gao, L. Xue, S. Xin, and J. B. Goodenough, "A High-Energy-Density Potassium Battery With a Polymer-Gel Electrolyte and a Polyaniline Cathode," *Angewandte Chemie International Edition* 57, no. 19 (2018): 5449–5453.

42. S. Wang, L. Zhang, Q. Zeng, et al., "Designing Polymer Electrolytes via Ring-Opening Polymerization for Advanced Lithium Batteries," *Advanced Energy Materials* 14, no. 3 (2024): 2302876.

43. A. Nishimoto, K. Agehara, N. Furuya, T. Watanabe, and M. Watanabe, "High Ionic Conductivity of Polyether-Based Network Polymer Electrolytes With Hyperbranched Side Chains," *Macromolecules* 32, no. 5 (1999): 1541–1548.

44. S. I. Lee, M. Schömer, H. Peng, et al., "Correlations Between Ion Conductivity and Polymer Dynamics in Hyperbranched Poly(Ethylene Oxide) Electrolytes for Lithium-Ion Batteries," *Chemistry of Materials* 23, no. 11 (2011): 2685–2688.

45. E. A. R. Zuiderveen, K. J. J. Kuipers, C. Caldeira, et al., "The Potential of Emerging Bio-Based Products to Reduce Environmental Impacts," *Nature Communications* 14, no. 1 (2023): 8521.

46. L. Liu, N. Solin, and O. Inganäs, "Bio Based Batteries," *Advanced Energy Materials* 11, no. 43 (2021): 2003713.

47. X. Zhu, J. C. Roy, X. Li, J. Li, and L. Zhang, "Toward Improved Sustainability in Lithium Ion Batteries Using Bio-Based Materials," *Trends in Chemistry* 5, no. 5 (2023): 393–403.

48. M. Rayung, M. M. Aung, S. C. Azhar, et al., "Bio-Based Polymer Electrolytes for Electrochemical Devices: Insight Into the Ionic Conductivity Performance," *Materials* 13, no. 4 (2020): 838.

49. S. Ahmed, P. Sharma, S. Bairagi, et al., "Nature-Derived Polymers and Their Composites for Energy Depository Applications in Batteries and Supercapacitors: Advances, Prospects and Sustainability," *Journal of Energy Storage* 66 (2023): 107391.

50. E. P. Feofilova and I. S. Mysyakina, "Lignin: Chemical Structure, Biodegradation, and Practical Application (A Review)," *Applied Biochemistry and Microbiology* 52, no. 6 (2016): 573–581.

51. H. Fei, Y. Liu, Y. An, et al., "Stable All-Solid-State Potassium Battery Operating at Room Temperature With a Composite Polymer Electrolyte and a Sustainable Organic Cathode," *Journal of Power Sources* 399 (2018): 294–298.

52. H. Liu, T. Xu, K. Liu, et al., "Lignin-Based Electrodes for Energy Storage Application," *Industrial Crops and Products* 165 (2021): 113425.

53. X. Meng, M. Poonia, C. G. Yoo, and A. J. Ragauskas, "Recent Advances in Synthesis and Application of Lignin Nanoparticles," in *Lignin Utilization Strategies: From Processing to Applications*, ed. C. G. Yoo and A. Ragauskas (American Chemical Society, 2021), 11–273.

54. A. T. Smit, E. Bellinetto, T. Dezaire, et al., "Tuning the Properties of Biobased PU Coatings via Selective Lignin Fractionation and Partial Depolymerization," *ACS Sustainable Chemistry & Engineering* 11, no. 18 (2023): 7193–7202.

55. E. Bellinetto, N. Fumagalli, M. Astorri, S. Turri, and G. Griffini, "Elucidating the Role of Lignin Type and Functionality in the Development of High-Performance Biobased Phenolic Thermoset Resins," *ACS Applied Polymer Materials* 6, no. 2 (2024): 1191–1203.

56. S. Trano, F. Corsini, G. Pascuzzi, et al., "Lignin as Polymer Electrolyte Precursor for Stable and Sustainable Potassium Batteries," *Chemsuschem* 15, no. 12 (2022): e202200294.

57. J. Han, A. Mariani, H. Zhang, et al., "Gelified Acetate-Based Water-In-Salt Electrolyte Stabilizing Hexacyanoferrate Cathode for Aqueous Potassium-Ion Batteries," *Energy Storage Materials* 30 (2020): 196–205.

58. L. Passauer, K. Fischer, and F. Liebner, "Activation of Pine Kraft Lignin by Fenton-Type Oxidation for Cross-Linking With Oligo (Oxyethylene) Diglycidyl Ether," *Holzforschung* 65 (2011): 319–326.

59. A. More, T. Elder, and Z. Jiang, "A Review of Lignin Hydrogen Peroxide Oxidation Chemistry With Emphasis on Aromatic Aldehydes and Acids," *Holzforschung* 75, no. 9 (2021): 806–823.

60. J. C. de Haro, E. Tatsi, L. Fagiolari, et al., "Lignin-Based Polymer Electrolyte Membranes for Sustainable Aqueous Dye-Sensitized Solar Cells," *ACS Sustainable Chemistry & Engineering* 9, no. 25 (2021): 8550–8560.

61. J. H. Park, H. H. Rana, J. Y. Lee, and H. S. Park, "Renewable Flexible Supercapacitors Based on All-Lignin-Based Hydrogel

Electrolytes and Nanofiber Electrodes," *Journal of Materials Chemistry A* 7, no. 28 (2019): 16962–16968.

62. L. Passauer, K. Fischer, and F. Liebner, "Preparation and Physical Characterization of Strongly Swellable Oligo (Oxyethylene) Lignin Hydrogel," *Holzforschung* 65 (2011): 309–317.

63. J. Clayden, N. Greeves, and S. Warren, *Organic Chemistry* (Oxford University Press, 2012).

64. Z. Xue, D. He, and X. Xie, "Poly(Ethylene Oxide)-Based Electrolytes for Lithium-Ion Batteries," *Journal of Materials Chemistry A* 3, no. 38 (2015): 19218–19253.

65. M. Jaipal Reddy, J. Siva Kumar, U. V. Subba Rao, and P. P. Chu, "Structural and Ionic Conductivity of PEO Blend PEG Solid Polymer Electrolyte," *Solid State Ionics* 177, no. 3 (2006): 253–256.

66. W. Lyu, X. Yu, Y. Lv, A. M. Rao, J. Zhou, and B. Lu, "Building Stable Solid-State Potassium Metal Batteries," *Advanced Materials* 36, no. 24 (2024): 2305795.

67. S. Chapi, M. V. Murugendrappa, A. Rayar, et al., "Enhanced Structural, Electrical, and Electrochemical Performance of Polyethylene Oxides (PEO)-Based Polymer Electrolytes for Solid State K+ Ion Batteries," *Journal of Applied Polymer Science* 141, no. 20 (2024): e55390.

68. G. Socrates, *Infrared and Raman Characteristic Group Frequencies: Tables and Charts* (John Wiley & Sons, 2004).

69. J. A. Baird, R. Olayo-Valles, C. Rinaldi, and L. S. Taylor, "Effect of Molecular Weight, Temperature, and Additives on the Moisture Sorption Properties of Polyethylene Glycol," *Journal of Pharmaceutical Sciences* 99, no. 1 (2010): 154–168.

70. C. M. Popescu, C. Vasile, M. C. Popescu, G. Singurel, V. Popa, and B. Munteanu, "Analytical Methods for Lignin Characterization. II. Spectroscopic Studies," *Cellulose Chemistry and Technology* 40 (2006): 597–621.

71. C. Allegretti, E. Bellinetto, P. D'Arrigo, et al., "Towards a Complete Exploitation of Brewers'; Spent Grain From a Circular Economy Perspective," *Fermentation* 8, no. 4 (2022): 8040151.

72. C. G. Boeriu, D. Bravo, R. J. A. Gosselink, and J. E. G. van Dam, "Characterisation of Structure-Dependent Functional Properties of Lignin With Infrared Spectroscopy," *Industrial Crops and Products* 20, no. 2 (2004): 205–218.

73. F. G. Calvo-Flores, J. A. Dobado, and F. J. M. M. Joaquín Isac-García, "Functional and Spectroscopic Characterization of Lignins," in *Lignin and Lignans as Renewable Raw Materials: Chemistry,Technology and Applications*, ed. F. G. Calvo-Flores, J. A. Dobado, J. Isac-García, and F. J. Martín-MartíNez (John Wiley & Sons, 2015), 145–188.

74. V. Passoni, C. Scarica, M. Levi, S. Turri, and G. Griffini, "Fractionation of Industrial Softwood Kraft Lignin: Solvent Selection as a Tool for Tailored Material Properties," *ACS Sustainable Chemistry & Engineering* 4, no. 4 (2016): 2232–2242.

75. P. Tanasini, G. Widmer, and R. Raballand, "Crosslinking and Decomposition of Epoxy Resins Induced by Contamination With Water–Assessment of an Industrial Scale Scenario," *Chemical Engineering Transactions* 48 (2016): 703–708.

76. Y. Noishiki and T. Miyata, "Polyepoxy Compound Fixation," in *Encyclopedia of Biomedical Polymers and Polymeric Biomaterials*, ed. M. Mishra, Vol. 11, 1st ed. (CRC Press, 2015), 9.

77. J. Leach, J. Wolinsky, P. Stone, and J. Wong, "Crosslinked α-Elastin Biomaterials: Towards a Processable Elastin Mimetic Scaffold," *Acta Biomaterialia* 1, no. 2 (2005): 155–164.

78. E. Cortés-Triviño, C. Valencia, M. A. Delgado, and J. M. Franco, "Modification of Alkali Lignin With Poly(Ethylene Glycol) Diglycidyl Ether to Be Used as a Thickener in Bio-Lubricant Formulations," *Polymers* 10, no. 6 (2018): 670.

79. V. Madhani, D. Kumar, D. K. Kanchan, and M. Singh Rathore, "Recent Advances and Prospects of K-Ion Conducting Polymer Electrolytes," *Journal of Electroanalytical Chemistry* 935 (2023): 117334.

80. K. Aruchamy, S. Ramasundaram, S. Divya, M. Chandran, K. Yun, and T. H. Oh, "Gel Polymer Electrolytes: Advancing Solid-State Batteries for High-Performance Applications," *Gels* 9, no. 7 (2023): 585.

81. R. Verma, P. N. Didwal, J. Y. Hwang, and C. J. Park, "Recent Progress in Electrolyte Development and Design Strategies for Next-Generation Potassium-Ion Batteries," *Batteries & Supercaps* 4, no. 9 (2021): 1428–1450.

82. H. Yin, C. Han, Q. Liu, F. Wu, F. Zhang, and Y. Tang, "Recent Advances and Perspectives on the Polymer Electrolytes for Sodium/Potassium-Ion Batteries," *Small* 17, no. 31 (2021): 2006627.

83. M. Zhu, J. Wu, Y. Wang, et al., "Recent Advances in Gel Polymer Electrolyte for High-Performance Lithium Batteries," *Journal of Energy Chemistry* 37 (2019): 126–142.

84. K. H. Chen, K. N. Wood, E. Kazyak, et al., "Dead Lithium: Mass Transport Effects on Voltage, Capacity, and Failure of Lithium Metal Anodes," *Journal of Materials Chemistry A* 5, no. 23 (2017): 11671–11681.

85. M. L. Lehmann, G. Yang, J. Nanda, and T. Saito, "Well-Designed Crosslinked Polymer Electrolyte Enables High Ionic Conductivity and Enhanced Salt Solvation," *Journal of the Electrochemical Society* 167, no. 7 (2020): 070539.

86. M. Dirican, C. Yan, P. Zhu, and X. Zhang, "Composite Solid Electrolytes for All-Solid-State Lithium Batteries," *Materials Science and Engineering: R: Reports* 136 (2019): 27–46.

87. M. A. Ratner, P. Johansson, and D. F. Shriver, "Polymer Electrolytes: Ionic Transport Mechanisms and Relaxation Coupling," *MRS Bulletin* 25, no. 3 (2000): 31–37.

88. Z. Wu, J. Zou, S. Shabanian, K. Golovin, and J. Liu, "The Roles of Electrolyte Chemistry in Hard Carbon Anode for Potassium-Ion Batteries," *Chemical Engineering Journal* 427 (2022): 130972.

89. Y. Lei, L. Qin, R. Liu, et al., "Exploring Stability of Nonaqueous Electrolytes for Potassium-Ion Batteries," *ACS Applied Energy Materials* 1, no. 5 (2018): 1828–1833.

90. H. Wang, D. Zhai, and F. Kang, "Solid Electrolyte Interphase (SEI) in Potassium Ion Batteries," *Energy & Environmental Science* 13, no. 12 (2020): 4583–4608.

91. M. Nishida, Y. Uraki, and Y. Sano, "Lignin Gel With Unique Swelling Property," *Bioresource Technology* 88, no. 1 (2003): 81–83.

92. D. Vural, J. C. Smith, and L. Petridis, "Polymer Principles Behind Solubilizing Lignin With Organic Cosolvents for Bioenergy," *Green Chemistry* 22, no. 13 (2020): 4331–4340.

Supporting Information

Additional supporting information can be found online in the Supporting Information section.